High-Rate Electrochemical Capacitors Based on Ordered Mesoporous Silicon Carbide-Derived Carbon

Yair Korenblit,[†] Marcus Rose,[‡] Emanuel Kockrick,[‡] Lars Borchardt,[‡] Alexander Kvit,[§] Stefan Kaskel,[‡,∥] and Gleb Yushin[†,*]

[†]School of Materials Science and Engineering, Georgia Institute of Technology, Atlanta, Georgia 30332, [‡]Department of Inorganic Chemistry, Dresden University of Technology, D-01062 Dresden, Germany, [§]Materials Science Center & Materials Science Department, University of Wisconsin-Madison, Madison, Wisconsin 53706, and [∥]Fraunhofer Institute Materials and Beam Technology, Dresden, Germany

ABSTRACT Microporous carbons, produced by selective etching of metal carbides in a chlorine-containing environment, offer narrow distribution of micropores and one of the highest specific capacitances reported when used in electrical double layer capacitors (EDLC) with organic electrolytes. Previously, the small micropores in these carbons served as an impediment to ion transport and limited the power storage characteristics of EDLC. Here we demonstrate, for the first time, how the preparation and application of templated carbide-derived carbon (CDC) can overcome the present limitations and show the route for dramatic performance enhancement. The ordered mesoporous channels in the produced CDC serve as ion-highways and allow for very fast ionic transport into the bulk of the CDC particles. The enhanced transport led to 85% capacitance retention at current densities up to ~20 A/g. The ordered mesopores in silicon carbide precursor also allow the produced CDC to exhibit a specific surface area up to 2430 m^2/g and a specific capacitance up to 170 F/g when tested in 1 M tetraethylammonium tetrafluoroborate solution in acetonitrile, nearly doubling the previously reported values.

KEYWORDS: carbide-derived carbon · SiC · porous · microporous · mesoporous · electrical double layer capacitor · electrochemical capacitor · supercapacitor · SBA-15

The development of advanced electrical double layer capacitors (EDLC) and improvement in the current understanding of the transport and adsorption phenomena of electrolyte ions within nanoporous carbon media has attracted much attention.[1−4] This is due to the increasing importance of EDLC technology for energy efficient industrial equipment, electric vehicles, and power grid applications.[5,6] While EDLC offer lower energy density than Li-ion batteries, they possess many attractive characteristics, not afforded by Li-ion batteries: operational life in excess of 500 000 charge−discharge cycles,[5−7] cost of power below $10/kW, and subminute charging.[5−7] Further improving the charge−discharge rate of EDLC without sacrificing their energy storage characteristics could be particularly important for leveling the subsecond disturbances in power lines, which cost billions of dollars to the world economy. In addition, faster charge and discharge would allow broader implementation of EDLC in military and aerospace applications. Batteries are still too slow for these applications while dielectric capacitors are too energy deficient and bulky.

The specific capacitance and energy storage characteristics of EDLC are strongly affected by the capability of carbon electrodes to adsorb a large quantity of ions under an applied potential[7] and attract the ions closer to the pore walls.[2,3,8] The power storage, or the charge−discharge time, of EDLC, in turn, is determined by how fast the ions can travel within the electrode particles.[7]

Most commercial EDLC employ activated carbon electrodes owing to their high specific surface area and thus relatively high specific capacitance values.[7] The activated carbons are produced from organic precursors and commonly exhibit a wide distribution of irregularly curved pores in the range of 0.3−4 nm,[9−13] often with narrow bottle-necks,[9,11−13] which may dramatically slow down the ion transport and thus limit the power characteristics of EDLC. An alternative method for porous carbon synthesis includes the use of inorganic precursors, such as carbides, and selective etching of noncarbon species. The resulting carbon is known as carbide-derived carbon (CDC).[10,14] The pore size of CDC can be very uniform.[10,15] This is due to the highly uniform distribution of carbon within such precursors and continuous extraction of large chloride molecules from CDC during their formation. These features prevent pore collapse and necking.[10] The absence of pores above 1 nm leads to higher capacitance values than that observed in traditional activated carbons due to, as recently

*Address correspondence to yushin@gatech.edu.

Received for review December 14, 2009 and accepted February 10, 2010.

Published online Xxxxxxxxx 00, 0000
10.1021/nn901825y

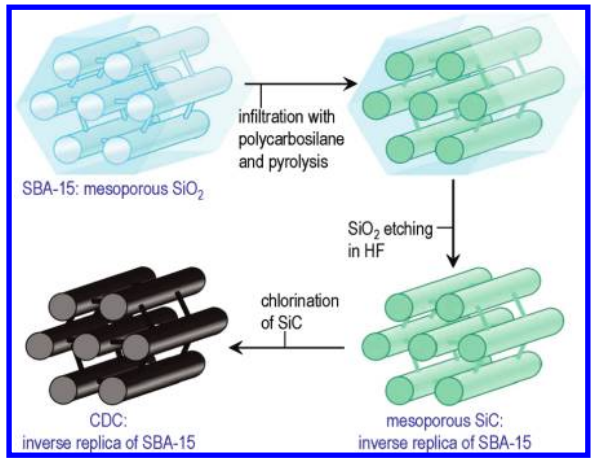

Figure 1. Schematic illustration of the fabrication of CDC with aligned mesopores.

discovered, the removal of the solvation shells from ions in subnanometer (<1 nm) pores and the resulting shorter charge-separation distances.[2,3] The adverse effect of the small pores in CDC exhibiting high capacitance is a relatively slow ion transport in small pores and thus a moderate rate of charge and discharge.[3,16] One of the potential approaches to boost the power performance of EDLC involves minimizing the ion paths within the microporous channels of porous carbons by decreasing the size of the porous carbon particles to submicrometer or, ideally, the nanorange. In a recent study of CDC produced from SiC and having different particle sizes (20 nm−20 μm) Portet *et al*. demonstrated improvements in the capacitance retention with high current density and a decrease of the time constant by up to ~33%.[17] While the study clearly demonstrated the potential for improved performance in porous carbon nanoparticles, the overall improvement of EDLC power characteristics was rather moderate, presumably due to the highly curved mesopores between the nanoparticles.[17] The straight pores of carbon nanotube (CNT) arrays[18] have demonstrated the potential for ultrafast transport of ions and triggered research on CNT-based EDLC.[19−22] However, CNT electrodes offer only a moderate specific capacitance due to their moderate surface area and the absence of subnanometer pores.[20,21]

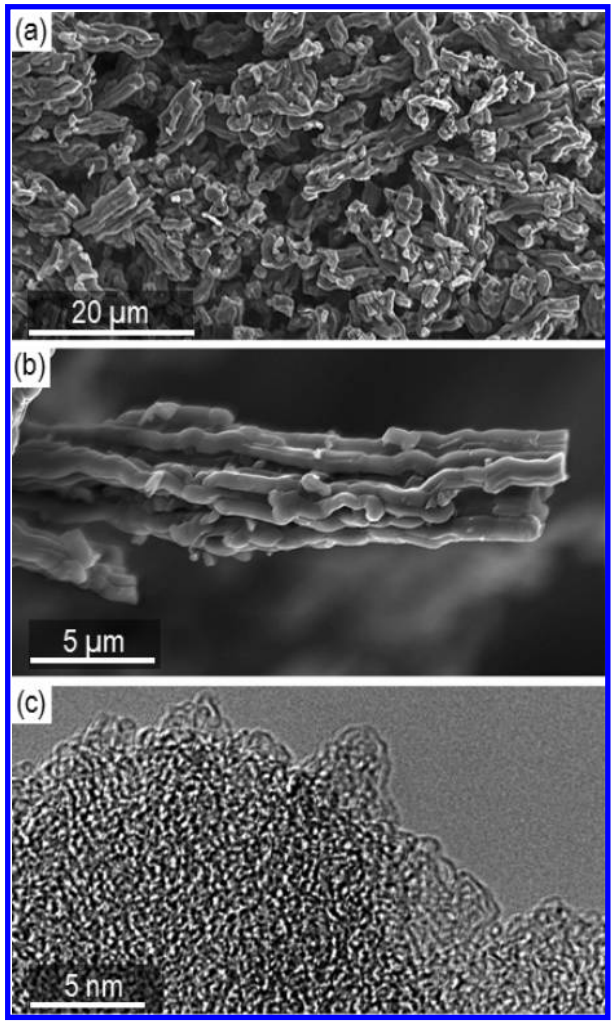

Figure 2. Electron microscopy of CDC samples: (a, b) SEM micrographs recorded at different magnification and showing the morphology of the produced particles; (c) high resolution TEM micrograph showing the microstructure of CDC.

Here we demonstrate the outstanding combination of ultrahigh specific capacitance, excellent frequency response, and capacity retention at high current densities of organic electrolyte EDLC based on novel CDC material having a combination of straight mesopore channels for fast ion transport and subnanometer pores in the volume between the large channels for high specific capacitance.

RESULTS AND DISCUSSION

Ordered mesoporous CDC material was prepared using a silicon carbide (SiC) precursor having ordered mesopores (Figure 1). Etching of silicon from SiC was achieved *via* the flow of Cl_2 gas at atmospheric pressure and a temperature of 700, 800, and 900 °C for 2 h according to the following reaction:[10,23]

$$SiC + 2Cl_2 \rightarrow SiCl_4 + C$$

While CDC produced from nonporous SiC micropowder requires at least 900 °C for complete chlorination,[10,17] mesoporous SiC powder can be completely transformed into CDC at temperatures below 700 °C. Since CDC formation from SiC is known to be a conformal process,[23] the shape and size of the produced CDC is expected to be very similar to that of the precursor SiC. The SiC was prepared using a high quality SBA-15 mesoporous SiO_2 template and polycarbosilane precursor. Figure 1 shows the process flow used for the fabrication of mesoporous CDC with aligned channels. Previously, the application of templates has been successfully demonstrated for the synthesis of activated carbons used in EDLC;[24,25] however, the formation of templated CDC is a novel process.

Figure 2 panels a and b show the morphology of

the CDC particles with elongated shape, 10−20 μm in length and 2−5 μm in diameter. Each particle commonly incorporates 5−20 smaller primary particles of comparable length but a smaller diameter in the range of 0.5−1 μm. This shape is typical for SBA-15[26] and its replicas[27] and is identical to the mesoporous SiC (Figure 1) produced prior to transformation to CDC (not shown). The transformation of SiC to C is known to be conformal at both the micrometer and the nanometer scales[23] and the observed conservation of shape was expected. High resolution TEM studies revealed the highly disordered microstructure of the produced CDC (Figure 2c), very similar to that observed in the prior studies of SiC-derived carbon.[17]

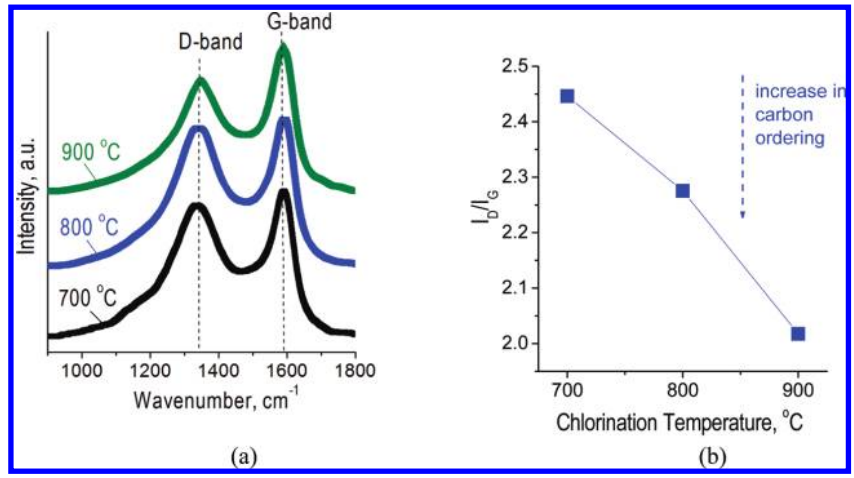

Figure 3. Microstructure of CDC samples: (a) Raman spectra and the corresponding (b) I_D/I_G ratio.

Raman spectroscopy confirmed the absence of unreacted SiC (not shown) and showed two broad peaks, typical for CDC and other disordered carbons (Figure 3a). The G-band, located at ~1590 cm^{-1} and corresponding to graphite in-plane vibrations, is slightly upshifted from 1582 cm^{-1},[28,29] which is common for CDC.[30,31] The disorder-induced D-band associated with a double-resonance Raman process in disordered carbon was located at ~1340 cm^{-1}.[28,29,32] The position of this band may vary, depending on the structure of the disordered carbon and the presence of impurities or functional groups.[32] The ratio of integrated intensities of the D-band and G-band (I_D/I_G) decreased with increasing chlorination temperature (Figure 3b). This observation suggests that ordering increases at higher chlorination temperatures, which is consistent with previous results on CDC.[10]

The N_2 sorption isotherms of all the mesoporous CDC samples are similar (Figure 4a). The accurate pore size analysis of porous carbons with a combination of micropores and small mesopores is a challenge, particularly when the shape of the pores at the micro- and meso- level is different. Classical Horvath−Kawazoe (HK)[33] and Saito−Foley (SF)[34] methods of N_2 sorption isotherm analysis produce erroneous results if microporous materials contain pores >1 nm.[35] Barrett−Joyner−Halenda (BJH)[36] and Dollimore−Heal (DH)[37] methods based on the Kelvin equation do not account for the effects of fluid−wall interactions, assume bulk-fluid-like behavior for pore adsorbate fluid, and fail to provide accurate analysis of nitrogen desorption isotherms for porous carbons containing micropores or small mesopores.[35] One of the most accurate methods for analyzing isotherms relies on calculations based on nonlocal density functional theory (DFT).[38,39] Unfortunately, DFT methods have only been developed for slit-shape, cylindrical, and mixed slit−cylindrical pore carbons. Furthermore, they assume dense graphitic pore walls. In our case, the mesopores between the CDC rods have different shape, and the mesopore walls are porous (Figure 1). For qualitative CDC pore size analysis we used the DFT model developed for slit-shape pores. While CDCs from nonporous microscopic SiC particles demonstrate no pores above 2 nm,[10,15] CDCs produced in this work at various temperatures show narrow distributions of mesopores in the range of 2−4 nm (Figure 4b). It is important to note, that when analyzing the adsorbate−adsorbent interaction potential, one needs all the atoms on the carbon surface adjacent to the N_2 molecule to be taken into consideration.[38,39] In the inverse cylindrical pores (pores between the cylinders) the sum of all the interactions between the N_2 adsorbate and the pore surface is weaker than that in slit-shape pores of the same size, because these interactions rapidly diminish with separation distance. Therefore the slit pore model used in our calculations is expected to show larger mesopores

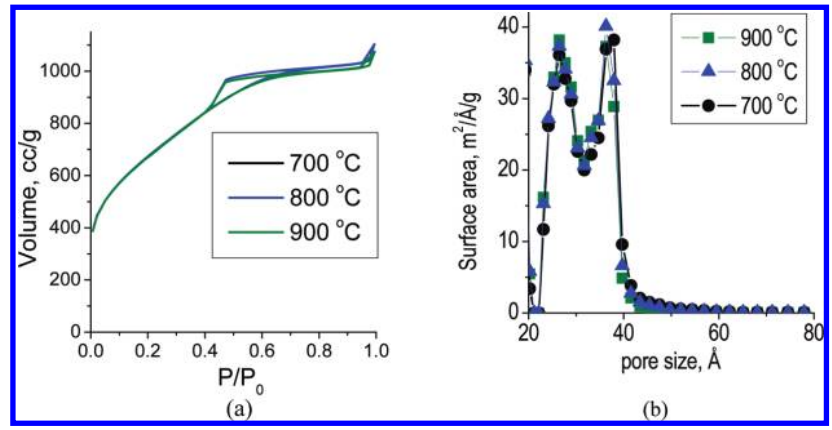

Figure 4. Porosity of CDC samples: (a) N_2 sorption isotherms recorded at 77 K on mesoporous CDC samples and (b) pore size distribution of aligned mesopores calculated using slit-pore DFT model.

TABLE 1. Porosity of SiC-Derived Carbon (CDC)

sample	particle size, μm	total pore volume, cc/g	BET SSA, m^2/g	DFT SSA of pores >2 nm, m^2/g	reference
mesoporous CDC, 700 °C	5−20	1.4	2250	490	this work
mesoporous CDC, 800 °C	5−20	1.5	2430	490	this work
mesoporous CDC, 900 °C	5−20	1.5	2420	480	this work
conventional CDC, 800−1100 °C	5−20	~0.5	1100−1200	13−40	10, 17
nanoparticle CDC, 800−1100 °C	0.02−0.03	1.8−2.2	1300−1310	220−260	10, 17

than actually present in CDC. However, we can assert that the distribution of mesopores in all the samples is very similar and that pores >4 nm are absent. These could be explained by the high quality of the template used and high conformality of the CDC process.[17]

Table 1 summarizes the porosity characteristics of our samples in comparison to CDC produced from nonporous SiC powder of 5−20 μm and 20−30 nm in size. While the specific surface area (SSA) calculated using the Brunauer−Emmett−Teller (BET) equation[40] may not be very accurate for microporous solids, it is still commonly used. The BET SSA of our CDC samples (2250−2430 m^2/g) are over two times higher than those obtained in prior studies of SiC-derived carbon[15,41] and among the highest ever reported for any CDC.[10,15,42] The very high external surface area of CDC nanorods (in excess of 1000 m^2/g for 3.5 nm rods, Figure 5), the more efficient removal of chloride molecules after the CDC synthesis due to the presence of aligned pores (Figure 1), and the greatly decreased probability of having completely closed pores due to the small CDC rod diameter are the likely contributors to the observed phenomena. The total pore volume of our mesoporous CDC (1.4−1.5 cc/g) is higher than that of microporous CDC (0.5 cc/g) but lower than that of CDC nanoparticles[17] (up to 2.2 cc/g) with mesopores between the agglomerated particles.

Small angle X-ray scattering (SAXS) studies confirmed the presence of aligned mesopores in the produced CDC. Interestingly, the distance between the ordered scattering centers (planes created by ordered CDC nanorods, Figure 1) varied depending on the synthesis conditions (Figure 6a). CDC samples produced during 700 °C chlorination showed the smallest separation distance of ~6.4 nm. Increasing chlorination temperature to 800 °C resulted in a separation distance of ~8.8 nm. Samples produced at 900 °C showed a major peak corresponding to 6.1 nm separations and a smaller peak corresponding to 10.5 nm separations. Since the size of the mesopores was similar for all the samples (Figure 4b) different SAXS peaks may indicate different diameters of the CDC nanorods and shrinkage of the CDC. Note that the SAXS spectra of mesoporous SiC prior to chlorination demonstrated a peak at ~8.8 nm, according to our studies (Figure 6b).

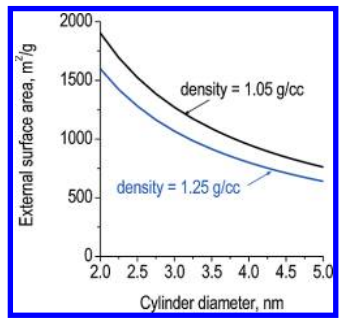

Figure 5. Theoretical calculations of the external specific surface area of CDC rods having density 1.05 and 1.25 g/cm^3 and diameter in the range of 2−5 nm.

The electrochemical tests of mesoporous CDC electrodes showed spectacular performance. Galvanostatic charge−discharge tests demonstrated a specific capacitance of up to 170 F/g at a current density of 100 mA/g (Figure 7a). To the best of our knowledge this is the highest capacitance ever reported for CDC and other carbons in the symmetric two-electrode configuration using tetraethylammonium tetrafluoroborate ($TEABF_4$)/acetonitrile electrolyte, which is used in most electrochemical capacitors produced in the U.S. It exceeds the specific capacitance of CDC produced from dense macroscopic SiC powder as well as that of most commercial activated carbons by nearly 100%. The highest performance was achieved in mesoporous CDC synthesized at the lowest temperature of 700 °C. The cause of the slightly lower than expected performance of the sample produced at 800 °C and exhibiting the highest BET SSA of 2430 m^2/g is not yet clear but may be related to the slight difference in the precursor synthesis procedure: the precursor for this sample contained additional carbon, which was added to improve the mesopore ordering and preserve the spacing between the CDC rods.[43] The procedure may have negatively affected the ionic transport and adsorption.

Lower chlorination temperatures of SiC commonly lead to both a lower degree of order in the structure (Figure 3) and higher capacitance, as previously reported.[3,17] The capacitance of many carbons normalized by the BET SSA often also show correlation with the (I_G/I_D) ratio,[21] which, in turn, may relate to the higher concentration of structural defects on the surface and the distortion of the solvation shells.[21] The ability of our process to achieve complete chlorination of SiC at lower temperature and allow for significantly enhanced BET SSA may have contributed to high values of the specific capacitance achieved. Interestingly, a recent report also suggested that the positive curvature found in one-

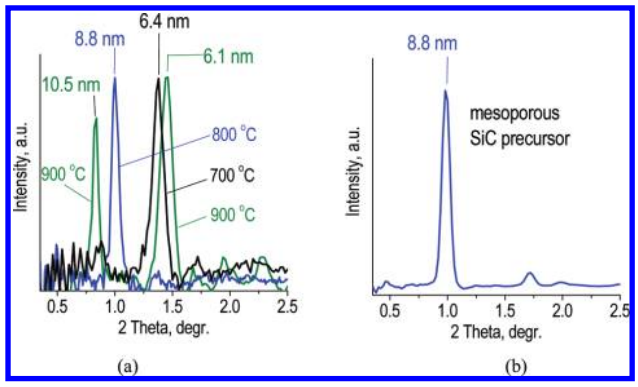

Figure 6. SAXS spectra of (a) CDC and (b) SiC precursor showing ordered mesopores. The background resulting from scattering on disordered features has been removed.

dimensional carbon nanotube arrays or zero-dimensional carbon onions, increases the normalized capacitance with decreasing tube diameter or particle size.[44] Therefore, the small diameter of CDC nanorods (Figure 1) may have also contributed to achieving relatively high capacitance on their external surface.

It is important to note that carbons produced by pyrolysis of organic precursors, which were infiltrated in the sacrificial SBA-15 templates commonly show moderate-to-low capacitance values.[24,25] Depending on the carbon precursor and synthesis conditions, SBA-15-templated carbons showed specific capacitance values in organic electrolytes in the range of 26−90 F/g,[24,25] which is two-to-five times lower than what is presently reported (Figure 7a). The difficulty in controlling the size of micropores in porous carbons prepared using common organic precursors limits their current performance characteristics since optimal distribution of micropores is critical for achieving high energy density EDLC electrodes.[3]

The aligned mesopores in CDC resulted in excellent capacitance retention at high discharge rates (Figure 4a). Mesoporous CDC produced at 700 °C showed specific capacitance of nearly 150 F/g for current densities exceeding 17000 mA/g (Figure 7a). Amazingly, with an increase in the current densities from ~1750 to 17500 mA/g, a very small decrease in capacitance of only ~2.5% was observed. In contrast, a popular activated carbon YP17D showed much stronger capacitance fading and a rather small capacitance of ~60 F/g at similarly high current densities. CDC produced from dense SiC particles and having no mesopores showed even worse performance, with specific capacitance continuously decreasing from ~90 to 67 F/g with current densities increasing to ~7000 mA/g. The performance of CDC nanoparticles was only slightly better than that of YP17D.

Electrochemical impedance spectroscopy allowed us to estimate the capacitance changes with the operating frequency (Figure 7b). The relative performance of all the carbons confirmed the result of charge−discharge tests and showed the highest capacitance and the best frequency response for the mesoporous CDC produced at 700 °C. The capacitance of microporous CDC does not show signs of saturation at 0.01 Hz, suggesting that larger particle size and thus longer diffusion paths for electrolyte ions prevent the system from reaching the equilibrium ion adsorption within a ~100 s time period. In contrast, most of the electrolyte ions reach the adsorption sites in the bulk of mesoporous CDC. We can approximate the highest operating frequency as the maximum frequency at which the capacitance decreases by no more than 50%. In comparison to CDC from dense SiC microparticles and activated carbon, mesoporous CDC exhibited nearly an order of magnitude better frequency response. While for strictly microporous CDC the maximum operating frequency was less than ~0.15 Hz, the operating frequency for CDCs having aligned mesopores exceeded 1 Hz. Such high operating frequency is rarely achieved in organic electrolytes.

The ability of the active materials to retain very high specific capacitance at high discharge rates results in excellent energy and power characteristics of EDLC. Figure 7c shows the Ragone plot of energy density *versus*

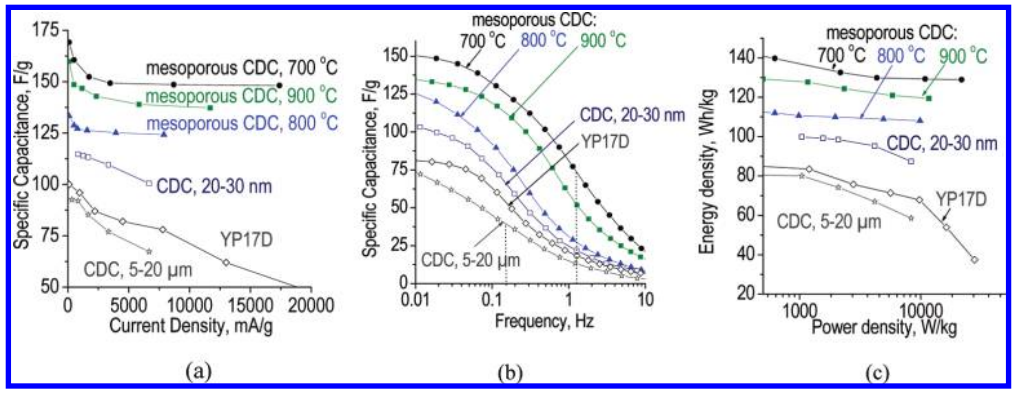

Figure 7. Electrochemical characterization of CDC with aligned mesopores produced at 700, 800, and 900 °C in comparison to that of activated carbon commonly used in commercial EDLC (YP17D) and CDC produced from micrometer-size and nano-size SiC powder at 900 °C: (a) capacitance retention with current density, (b) frequency response of capacitance, and (c) Ragone plot of energy density *vs* power density.

power density of active material for all the carbons under study. Mesoporous CDCs clearly demonstrate significantly higher energy and power characteristics than microporous CDCs and activated carbon.

CONCLUSION

The preparation and application of templated CDC overcame the present limitations of slow intraparticle ion transport and poor control over the bimodal pore size distribution in the carbons currently used, and showed a route for further performance enhancement. The ordered mesoporous channels in SiC CDC serve as ion-highways and allow for very fast ionic transport into the bulk of the CDC particles, thus leading to an excellent frequency response and outstanding capacitance retention at high current densities. The ordered mesopores in SiC allowed for a greatly increased SSA and specific capacitance of SiC CDC, nearly doubling the previously reported values.[17] The use of CDC produced from other carbides, including mesoporous TiC or VC is expected to further enhance the energy storage characteristics of EDLC electrodes, while optimization of the mesopore size is expected to enhance the power characteristics of EDLC.

MATERIALS AND METHODS

Material Preparation. A mesoporous, high quality, SBA-15 SiO_2 template with uniform network porosity and wall thickness was used for the nanocasting process. According to the employed procedure[45,43] (for 700 and 800 °C), 2 g of SBA-15 were infiltrated with 2.5 g of polycarbosilane precursor solution (M_w = 800 from Aldrich) in a heptane−butanol mixture in an open beaker and left to evaporate overnight while stirring. The resulting powder was then placed in an alumina boat in a tube furnace under Ar flowing at the rate of ~40 mL min^{-1} and heated to 1000 °C according to the following regime: (a) heating from room temp to 300 °C at the rate of 2.5 °C/min, (b) 5 h heat treatment at 300 °C, (c) heating from 300 to 700 °C at the rate of 0.5 °C/min, (d) heating from 700 to 1000 at 2 °C/min, (e) annealing at 1000 °C for 2 h, and (f) cooling down to room temperature.

The samples prepared at 800 °C used a precursor that was prepared slightly differently: (a) additional carbon was added to the SBA-15 template by infiltration of divinylbenzene in addition to the polycarbosilane (SMP-10 from Starfire), which was kept under vacuum at ambient temperature overnight. Also, the samples were (b) heated under Ar atmosphere to 300 °C at ~2.5 °C/min, (c) annealed at 300 °C for 5 h under Ar atmosphere, (d) heated from 300 to 700 °C in Ar at 0.5 °C/min, (e) directly heated from 700 to 1000 at 2 °C/min, (f) annealed at 1000 °C for 2 h, and (g) cooled down to room temperature. The microstructure and porosity of the mesoporous SiC samples produced according to the two methods were similar.

The silicon in the SiC was removed using a high temperature chlorination treatment. Therefore the samples were heated at 7.5 °C/min up to 700, 800, and 900 °C, respectively. The duration of annealing under a dynamic chlorine atmosphere was 2 h for all three samples. The samples were treated in ammonia at 600 °C for 3 h to remove residual chlorine from the highly porous material.

The carbon powders were suspended in ethanol and mixed with polytetrafluoroethylene (PTFE) (60 wt % water suspension, Sigma Aldrich) binder to form a slurry consisting of 95 wt % carbon and 5 wt % PTFE. In addition to CDC, an activated carbon sample (YP17D, Kuraray Chemical, Osaka, Japan) was used for performance comparison. Once most of the ethanol was evaporated under continuous stirring at 300 rpm and 100 °C, the material was further mixed using a spatula until a soft clay-like consistency was achieved, and the resulting composite paste was made into a thin, rubbery film, and used as electrodes. After drying overnight at 80 °C under vacuum, the electrode peel was rolled to the thickness of ~150 μm using a commercial rolling mill and left to dry in the vacuum oven at 80 °C for at least 8 h until the EDLC device with organic electrolyte was constructed and used for electrochemical testing.

Device Assembly. The EDLC were assembled in a symmetrical two-electrode configuration. Al foil of 300 μm in thickness was roughened using a 600 grit SiC sandpaper, coated by a thin layer (~10 to 20 μm) of conductive paint (EB-012, Acheson Colloids) and used as a current collector. The conductive paint was used to reduce the interfacial resistance between the electrode and the current collector. A GORE membrane (W.L. Gore and Associates) of ~25 μm in thickness and ~60% porosity was used as a separator for the EDLC devices. The Al−electrode−separator−electrode−Al sandwich was clamped between two Teflon slabs and transferred into the Ar-filled glovebox (Innovative technologies, <1 ppm of H_2O). After being allowed to outgas in a glovebox vacuum oven at 120 °C for 2 h, the whole assembly was cooled down to room temperature, placed in a glass beaker, and filled with an organic electrolyte. We selected 1 M tetraethylammonium tetrafluoroborate salt (electrochemical grade, Alfa Aesar) solution in acetonitrile (99.9%, extra dry, Across Organics, Geel, Belgium). Prior to electrolyte preparation, $TEABF_4$ salt was dried for 2 h at 150 °C in a vacuum oven located inside the glovebox. The beaker-type EDLC device was placed into a custom designed airtight glass cell equipped with two Swagelok electrical feedthroughs and taken out of the glovebox for electrochemical characterization.

Testing. Electrochemical characterization of the materials synthesized entailed charge−discharge (C−D) and electrochemical impedance spectroscopy (EIS). The EIS tests were carried out using a Zahner IM6 electrochemical workstation (Zahner-Elektrik Gmbh & CoGK, Kronach, Germany) in the frequency range of 10 mHz−100 kHz with a 10 mV AC amplitude. The gravimetric capacitance, C (F/g), was calculated according to

$$C = \frac{2}{2\pi f \mathrm{Im}(Z) m}$$

where f is the operating frequency (Hz), Im(Z) is the imaginary part of the total device resistance (ohm), and m is the mass of carbon in each electrode (g).

The C−D tests were carried out using an Arbin SCTS supercapacitor testing system (Arbin Instruments, TN) between 0 and +2 V at charge/discharge current densities between 100 and 15000 mA/g, based on the mass of a single electrode. The gravimetric capacitance, C (F/g), was calculated according to

$$C = \frac{2I}{(dV/dt)m}$$

where I is the current (A), dV/dt is the slope of the discharge curve (V/s), and m is the mass of carbon in each electrode (g).

The energy density, E (W · h/kg), of the electrodes was estimated as

$$E = \frac{CV^2}{2} 1000\ (\mathrm{g/kg}) \frac{1}{3600} (\mathrm{W{\cdot}h/J})$$

where C is gravimetric capacitance of the electrode (F/g) calculated from C−D tests at different current densities, V is the EDLC operating voltage (V). The power density, P (W/kg), of the electrodes was calculated by dividing the electrode energy density by the EDLC discharge time (h) at different current densities.

The isotherms of N_2 gas adsorption on the surface of CDC powders were collected at 77 K in the range of relative pressures of 0.05−1 P/P_0 using TriStar II 3020 surface area and poros-

ity measurement system (Micromeritics Inc., GA) and used for measurements of the SSA and pore size distribution (PSD) in the mesopore range (2−50 nm). The SSA and PSD were calculated using the BET and DFT methods, respectively. Both the BET and DFT analyses were performed using Micromeritics software. The DFT model assumed slit-pore shape. The relative pressure range of P/P_0 from 0.05 to 0.2 was used for multipoint BET calculations. Ultra high purity gases (99.99%, Airgas) were used for all experiments.

Micro-Raman spectroscopy was performed using an Ar ion laser excitation (488 nm) on a Ramascope 1000 Raman microspectrometer (Renishaw, UK) equipped with a charged coupled device (CCD) detector and an optical microscope for focusing the incident laser beam to a 1−2 μm spot size. The spectra were collected in the extended regime in the range of 800−1800 cm^{-1}. Prior to analysis, the microspectrometer was calibrated using a plain Si wafer. Small angle X-ray scattering (SAXS) experiments were performed on Nanostar (Bruker, Madison) equipped with HiStar 2D detector. Scanning electron microscopy (SEM) was performed using a LEO 1530 SEM microscope (LEO, Osaka, Japan, now Nano Technology Systems Division of Carl Zeiss SMT, MA). An in-lens secondary electron detector was used for the studies, most of which were performed using an accelerating voltage of 5 kV and a working distance of 5 mm. Transmission electron microscopy (TEM) observations of CDC microstructure were carried out using a Philips CM200UT microscope (Philips, Netherlands) operated at an accelerating voltage of 200 kV.

Acknowledgment. This work was partially supported by AFOSR Grant No. FA9550-09-1-0176.

REFERENCES AND NOTES

1. Raymundo-Pinero, E.; Kierzek, K.; Machnikowski, J.; Beguin, F. Relationship between the Nanoporous Texture of Activated Carbons and Their Capacitance Properties in Different Electrolytes. *Carbon* **2006**, *44*, 2498–2507.
2. Chmiola, J.; Largeot, C.; Taberna, P. L.; Simon, P.; Gogotsi, Y. Desolvation of Ions in Subnanometer Pores and Its Effect on Capacitance and Double-Layer Theory. *Angew. Chem., Int. Ed.* **2008**, *47*, 3392–3395.
3. Chmiola, J.; Yushin, G.; Gogotsi, Y.; Portet, C.; Simon, P. Anomalous Increase in Carbon Capacitance at Pore Size Below 1 nm. *Science* **2006**, *313*, 1760–1763.
4. Nishihara, H.; Itoi, H.; Kogure, T.; Hou, P. X.; Touhara, H.; Okino, F.; Kyotani, T. Investigation of the Ion Storage/Transfer Behavior in an Electrical Double-Layer Capacitor by Using Ordered Microporous Carbons as Model Materials. *Chem.—Eur. J.* **2009**, *15*, 5355–5363.
5. Simon, P.; Gogotsi, Y. Materials for Electrochemical Capacitors. *Nat. Mater.* **2008**, *7*, 845–854.
6. Miller, J. R.; Simon, P. Materials Science—Electrochemical Capacitors for Energy Management. *Science* **2008**, *321*, 651–652.
7. Conway, B. E. *Electrochemical Supercapacitors*; Kluwer Academic/Plenum Publishers: New York, 1999; Vol. 1, p 698.
8. Huang, J. S.; Sumpter, B. G.; Meunier, V. Theoretical Model for Nanoporous Carbon Supercapacitors. *Angew. Chem., Int. Ed.* **2008**, *47*, 520–524.
9. Barton, T. J.; Bull, L. M.; Klemperer, W. G.; Loy, D. A.; McEnaney, B.; Misono, M.; Monson, P. A.; Pez, G.; Scherer, G. W.; Vartuli, J. C.; *et al.* Tailored Porous Materials. *Chem. Mater.* **1999**, *11*, 2633–2656.
10. Yushin, G.; Gogotsi, Y.; Nikitin, A. Carbide Derived Carbon. In *Nanomaterials Handbook*; Gogotsi, Y., Ed.; CRC Press: Boca Raton, FL, 2006; pp 237−280.
11. Kyotani, T. Control of Pore Structure in Carbon. *Carbon* **2000**, *38*, 269–286.
12. Kaneko, K. Determination of Pore Size and Pore Size Distribution. Adsorbents and Catalysts. *J. Membr. Sci.* **1994**, *96*, 59–89.
13. Saufi, S. M.; Ismail, A. F. Fabrication of Carbon Membranes for Gas Separation—A Review. *Carbon* **2004**, *42*, 241–259.
14. Janes, A.; Lust, E. Electrochemical Characteristics of Nanoporous Carbide-Derived Carbon Materials in Various Nonaqueous Electrolyte Solutions. *J. Electrochem. Soc.* **2006**, *153*, A113–A116.
15. Yushin, G.; Dash, R. K.; Gogotsi, Y.; Jagiello, J.; Fischer, J. E. Carbide-Derived Carbons: Effect of Pore Size on Hydrogen Uptake and Heat of Adsorption. *Adv. Funct. Mater.* **2006**, *16*, 2288–2293.
16. Chmiola, J.; Yushin, G.; Dash, R. K.; Hoffman, E. N.; Fischer, J. E.; Barsoum, M. W.; Gogotsi, Y. Double-Layer Capacitance of Selected Carbide Derived Carbons in Sulfuric Acid. *Electrochem. Solid State Commun.* **2005**, *8*, A357–A360.
17. Portet, C.; Yushin, G.; Gogotsi, Y. Effect of Carbon Particle Size on Electrochemical Performance of EDLC. *J. Electrochem. Soc.* **2008**, *155*, A531–A536.
18. Turano, S. P.; Ready, J. Chemical Vapor Deposition Synthesis of Self-Aligned Carbon Nanotube Arrays. *J. Electron. Mater.* **2006**, 192–194.
19. Frackowiak, E.; Beguin, F. Electrochemical Storage of Energy in Carbon Nanotubes and Nanostructured Carbons. *Carbon* **2002**, *40*, 1775–1787.
20. Niu, C. M.; Sichel, E. K.; Hoch, R.; Moy, D.; Tennent, H. High Power Electrochemical Capacitors Based on Carbon Nanotube Electrodes. *Appl. Phys. Lett.* **1997**, *70*, 1480–1482.
21. Portet, C.; Yushin, G.; Gogotsi, Y. Electrochemical Performance of Carbon Onions, Nanodiamonds, Carbon Black and Multiwalled Nanotubes in Electrical Double Layer Capacitors. *Carbon* **2007**, *45*, 2511–2518.
22. An, K. H.; Kim, W. S.; Park, Y. S.; Choi, Y. C.; Lee, S. M.; Chung, D. C.; Bae, D. J.; Lim, S. C.; Lee, Y. H. Supercapacitors Using Single-Walled Carbon Nanotube Electrodes. *Adv. Mater.* **2001**, *13*, 497–500.
23. Cambaz, Z. G.; Yushin, G. N.; Vyshnyakova, K. L.; Pereselentseva, L. N.; Gogotsi, Y. G. Formation of Carbide-Derived Carbon on Beta-Silicon Carbide Whiskers. *J. Am. Ceram. Soc.* **2006**, *89*, 509–514.
24. Jurewicz, K.; Vix-Guterl, C.; Frackowiak, E.; Saadallah, S.; Reda, A.; Parmentier, J.; Patarin, J.; Beguin, F. Capacitance Properties of Ordered Porous Carbon Materials Prepared by a Templating Procedure. *J. Phys. Chem. Solids* **2004**, *65*, 287–293.
25. Zhou, H. S.; Zhu, S. M.; Hibino, M.; Honma, I. Electrochemical Capacitance of Self-Ordered Mesoporous Carbon. *J. Power Sources* **2003**, *122*, 219–223.
26. Zhao, D. Y.; Feng, J. L.; Huo, Q. S.; Melosh, N.; Fredrickson, G. H.; Chmelka, B. F.; Stucky, G. D. Triblock Copolymer Syntheses of Mesoporous Silica with Periodic 50 to 300 Angstrom Pores. *Science* **1998**, *279*, 548–552.
27. Liu, X. W.; Zhou, L.; Li, J. W.; Sun, Y.; Su, W.; Zhou, Y. P. Methane Sorption on Ordered Mesoporous Carbon in the Presence of Water. *Carbon* **2006**, *44*, 1386–1392.
28. Tuinstra, F.; Koenig, J. L. Raman Spectrum of Graphite. *J. Chem. Phys.* **1970**, *53*, 1126–1130.
29. Nemanich, R. J.; Solin, S. A. 1st-Order and 2nd-Order Raman-Scattering from Finite-Size Crystals of Graphite. *Phys. Rev. B* **1979**, *20*, 392–401.
30. Portet, C; Korenblit, Y.; Gogotsi, Y.; Mokaya, R.; Yushin, G. Electrical Double Layer Capacitance of Zeolite-Templated Carbon in Organic Electrolyte. *J. Electrochem. Soc.* **2009**, *156*, A1–A6.
31. Yushin, G.; Hoffman, E.; Nikitin, A.; Ye, H.; Barsoum, M. W.; Gogotsi, Y. Synthesis of Nanoporous Carbide-Derived Carbon by Chlorination of Titanium Silicon Carbide. *Carbon* **2005**, *44*, 2075–2082.
32. Ferrari, A. C.; Robertson, J. Raman Spectroscopy of Amorphous, Nanostructured, Diamond-like Carbon, and Nanodiamond. *Phil. Trans. R. Soc. A* **2004**, *362*, 2477–2512.
33. Horvath, G.; Kawazoe, K. Method for the Calculation of Effective Pore-Size Distribution in Molecular-Sieve Carbon. *J. Chem. Eng. Jpn.* **1983**, *16*, 470–475.
34. Saito, A.; Foley, H. C. Curvature and Parametric Sensitivity in Models for Adsorption in Micropores. *AIChE J.* **1991**, *37*, 429–436.

35. Yang, R. T. *Adsorbents: Fundamentals and Applications*; Wiley & Sons, Inc.: Hoboken, NJ, 2003.
36. Barrett, E. P.; Joyner, L. G.; Halenda, P. P. The Determination of Pore Volume and Area Distributions in Porous Substances. 1. Computations from Nitrogen Isotherms. *J. Am. Chem. Soc.* **1951**, *73*, 373–380.
37. Dollimore, D.; Heal, G. R. Improved Method for Calculation of Pore Size Distribution from Adsorption Data. *J. Appl. Chem. USSR* **1964**, *14*, 109.
38. Ravikovitch, P. I.; Neimark, A. V. Characterization of Nanoporous Materials from Adsorption and Desorption Isotherms. *Colloids Surf., A* **2001**, *187−188*, 11–21.
39. Ravikovitch, P. I.; Vishnyakov, A.; Russo, R.; Neimark, A. V. Unified Approach to Pore Size Characterization of Microporous Carbonaceous Materials from N-2, Ar, and CO_2 Adsorption Isotherms. *Langmuir* **2000**, *16*, 2311–2320.
40. Brunauer, S.; Emmett, P.; Teller, E. Adsorption of Gases in Multimolecular Layers. *J. Am. Chem. Soc.* **1938**, *60*, 309–319.
41. Portet, C.; Yushin, G.; Gogotsi, Y. Effect of Carbon Particle Size on Electrochemical Performance of EDLC. *J. Electrochem. Soc.* **2008**, *155*, A531−A536.
42. Yushin, G.; Hoffman, E. N.; Barsoum, M. W.; Gogotsi, Y.; Howell, C. A.; Sandeman, S. R.; Phlllips, G. J.; Lloyd, A. W.; Mikhalovsky, S. V. Mesoporous Carbide-Derived Carbon with Porosity Tuned for Efficient Adsorption of Cytokines. *Biomaterials* **2006**, *27*, 5755–5762.
43. Krawiec, P.; Kockrick, E.; Borchardt, L.; Geiger, D.; Corma, A.; Kaskel, S. Ordered Mesoporous Carbide Derived Carbons: Novel Materials for Catalysis and Adsorption. *J. Phys. Chem. C* **2009**, *113*, 7755–7761.
44. Huang, J. S.; Sumpter, B. G.; Meunier, V.; Yushin, G.; Portet, C.; Gogotsi, Y. Curvature Effects in Carbon Nano-Materials: Exohedral Versus Endohedral Supercapacitors. *J. Mater. Res.* **2009**, (in press).
45. Kockrick, E.; Krawiec, P.; Petasch, U.; Martin, H. P.; Herrmann, M.; Kaskel, S. Porous CeO_x/SiC Nanocomposites Prepared from Reverse Polycarbosilane-Based Microemulsions. *Chem. Mater.* **2008**, *20*, 77–83.